J. Fluid Mech. (2001), *vol.* 435, *pp.* 397–407. Printed in the United Kingdom

© 2001 Cambridge University Press

Self-similar shedding of vortex rings

By MONIKA NITSCHE

Department of Mathematics and Statistics, University of New Mexico, Albuquerque, NM 87131, USA

(Received 4 December 2000 and in revised form 25 January 2001)

The roll-up of an initially spherical vortex sheet into a vortex ring is computed using the vortex blob method. The ring sheds about 30% of its circulation into a tail which, in turn, rolls up into a ring that sheds circulation. The process repeats itself at smaller and smaller scales in a self-similar manner. The relation between the vortex shedding and the energy of the vortices is investigated. In contrast, an initially cylindrical vortex sheet rolls up into a vortex pair that sheds essentially no circulation.

1. Introduction

Consider a sphere immersed in stagnant inviscid fluid which is impulsively set into motion. The resulting potential flow is induced by an axisymmetric vortex sheet in place of the sphere. This paper studies the evolution of the vortex sheet under its self-induced velocity, as if the sphere were dissolved and the fluid within it allowed to move with the flow. The axisymmetric flow is compared to the planar flow generated by the impulsive motion of a cylinder. Rottman, Simpson & Stansby (1987) performed an experiment simulating the cylindrical scenario by quickly removing a hollow cylinder immersed in a crossflow. They also computed this flow using a vortex-in-cell method and compared numerical and experimental results. Rottman & Stansby (1993) computed the planar flow using the vortex blob method. The axisymmetric flow was computed by Winckelmans *et al.* (1995) using a three-dimensional vortex particle method.

Here, we compute the planar and axisymmetric flow to longer times than in prior work, using the vortex blob method. The method consists of regularizing the singular governing equations by introducing an artificial parameter δ (Chorin & Bernard 1973; Anderson 1985; Krasny 1986). Comparisons with solutions of the Navier–Stokes equations (Tryggvason, Dahm & Sbeih 1991) and with experimental measurements (Nitsche & Krasny 1994) show that the method approximates viscous flow well for sufficiently small values of the artificial smoothing parameter and viscosity.

The computed planar and axisymmetric sheets roll up into a vortex pair and a vortex ring respectively as they travel in the direction of the given impulse. However, the vortex ring sheds about 30% of its circulation into a tail which, in turn, rolls up into a vortex ring. This observed shedding and roll-up repeats itself in a self-similar manner, forming a sequence of vortex rings of decreasing size in the tail of the leading ring. In contrast, the vortex pair does not shed any significant amount of circulation. The results are shown to be essentially independent of the flow regularization. The relation between the observed shedding and the energy of the vortex rings is also discussed, motivated by the work of Gharib, Rambod & Shariff (1998) relating the energy and the circulation of vortex rings generated in laboratory experiments.

The paper is organized as follows. Section 2 describes the initial conditions and the governing equations. Section 3 presents the computed vortex sheet roll-up and discusses the vortex shedding process. The results are summarized in § 4.

2. Problem formulation

2.1. *Initial conditions*

Let (x, y, z) be a Cartesian coordinate system such that the initially cylindrical and spherical sheets are centred at the origin and the z-axis equals the axis of the cylinder. The impulsively given initial velocity is $(U, 0, 0)$. The radius of the cylinder and sphere is a. The vortex sheets at time t are described by their cross-section with the upper (x, y)-plane $(x(\alpha, t), y(\alpha, t))$, and by their circulation distribution $\Gamma(\alpha)$. Here, α is a Lagrangian parameter chosen to be the initial angular coordinate in the (x, y)-plane. The circulation is obtained by integrating the jump in the tangential velocity across the sheet, σ, with respect to arclength, s. From the initial streamfunction (Batchelor 1967, §§ 6.6, 6.8) it follows that

$$\sigma_{2d}(s, 0) = 2U \sin\alpha, \quad \sigma_{3d}(s, 0) = \tfrac{3}{2} U \sin\alpha, \quad s = a\alpha, \quad 0 \leqslant \alpha \leqslant \pi, \tag{2.1}$$

and $\Gamma(\alpha) = \int_0^{s(\alpha)} \sigma(s, 0) \mathrm{d}s$ is obtained accordingly. Here, $2d$ and $3d$ refer to the planar and axisymmetric case respectively.

The total circulation in the upper half of the (x, y)-plane, $\Gamma_T = \Gamma(\pi)$, is

$$\Gamma_{T,2d} = 4Ua, \qquad \Gamma_{T,3d} = 3Ua. \tag{2.2}$$

The flow is non-dimensionalized with respect to the total circulation Γ_T and the initial radius a. With this choice, the initial conditions are given by

$$x(\alpha, 0) = \cos\alpha, \quad y(\alpha, 0) = \sin\alpha, \quad \Gamma(\alpha) = (1 - \cos\alpha)/2, \quad 0 \leqslant \alpha \leqslant \pi. \tag{2.3}$$

The corresponding non-dimensional velocity U is $U_{2d} = 1/4$, $U_{3d} = 1/3$.

2.2. *Evolution equation*

The vortex sheet is a superposition of vortex elements with strength $\mathrm{d}\Gamma = \Gamma'(\alpha)\mathrm{d}\alpha$. The planar and axisymmetric elements are counter-rotating pairs of vortex lines and circular vortex filaments respectively. The regularized streamfunction at (x, y) induced by an element at $(\tilde{x}, \tilde{y})$ of unit strength is

$$\psi_{2d}(x, y, \tilde{x}, \tilde{y}) = -\frac{1}{4\pi} \log \frac{(x - \tilde{x})^2 + (y - \tilde{y})^2 + \delta^2}{(x - \tilde{x})^2 + (y + \tilde{y})^2 + \delta^2}, \tag{2.4a}$$

$$\psi_{3d}(x, y, \tilde{x}, \tilde{y}) = \frac{y\tilde{y}}{4\pi} \int_0^{2\pi} \frac{\cos\theta}{(\rho^2 + \delta^2)^{1/2}} \, \mathrm{d}\theta, \tag{2.4b}$$

where $\rho^2 = (x - \tilde{x})^2 + y^2 + \tilde{y}^2 - 2\, y\, \tilde{y} \cos\theta$ and δ is the regularization parameter. The global streamfunction for the vortex sheet is obtained by superposition,

$$\psi(x, y, t) = \int_0^{\pi} \psi(x, y, x(\alpha, t), y(\alpha, t))\, \Gamma'(\alpha) \, \mathrm{d}\alpha. \tag{2.5}$$

The induced velocities are obtained from the streamfunction,

$$(u, v)_{2d} = \left(\frac{\partial\psi}{\partial y}, -\frac{\partial\psi}{\partial x} \right), \quad (u, v)_{3d} = \left(\frac{1}{y}\frac{\partial\psi}{\partial y}, -\frac{1}{y}\frac{\partial\psi}{\partial x} \right), \tag{2.6}$$

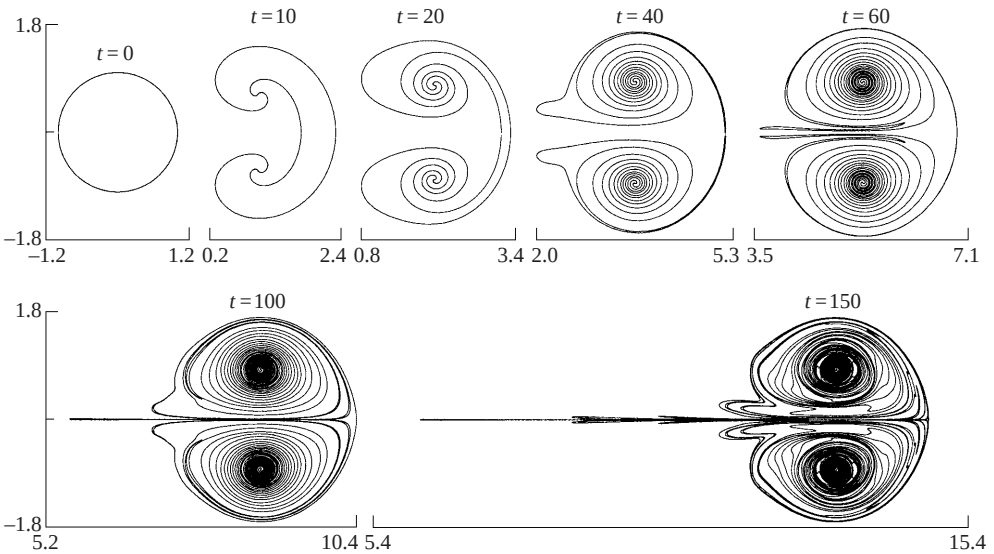

FIGURE 1. Computed planar solution at the indicated times, using $\delta = 0.2$.

and the sheets evolve under self-induction

$$\frac{\mathrm{d}x}{\mathrm{d}t}(\alpha, t) = u(x(\alpha, t), y(\alpha, t), t), \qquad \frac{\mathrm{d}y}{\mathrm{d}t}(\alpha, t) = v(x(\alpha, t), y(\alpha, t), t), \tag{2.7}$$

with the given initial conditions (2.3). The figures in the next section plot the computed solution $(x(\alpha, t), y(\alpha, t))$, $0 \leqslant \alpha \leqslant \pi$, together with its image in the lower (x, y)-plane.

2.3. *Numerical method*

The sheets are discretized by mesh points (x_j, y_j), $j = 1, \ldots, N$, corresponding to an initially uniform discretization in the parameter α. The points satisfy a system of ordinary differential equations obtained by evaluating the integrals on the right-hand side of equation (2.7) using the trapezoid rule. The system is integrated in time with the fourth-order Runge–Kutta method. As the vortex sheets roll up and stretch, additional mesh points are inserted to maintain resolution (Krasny 1987).

3. Numerical results

3.1. *Vortex sheet roll-up*

Figure 1 plots the evolution of the initially cylindrical vortex sheet at the indicated times, computed with $\delta = 0.2$. The sheet rolls up into two counter-rotating spirals as it travels in the direction of the given impulse. The vorticity is maximal at the spiral centre and the roll-up approximates a vortex pair. At $t = 40$, a portion of the sheet forms a lip at the rear of the vortex. One might expect this lip to stay behind the vortex at later times, but instead it is mostly entrained and moves with the vortex. At $t = 150$, only 1.5% of the total vorticity stays behind in the shape of a thin tail. Note that this tail stems in part from the observed lip, and in part from folds in the outer vortex sheet turns visible at $t = 100$ and $t = 150$. However, the folds contain almost no vorticity and do not contribute significantly to the tail vorticity.

Figure 2 plots the evolution of the initially spherical vortex sheet at the indicated times, computed with $\delta = 0.2$. As in the planar case, the vortex sheet rolls up as it

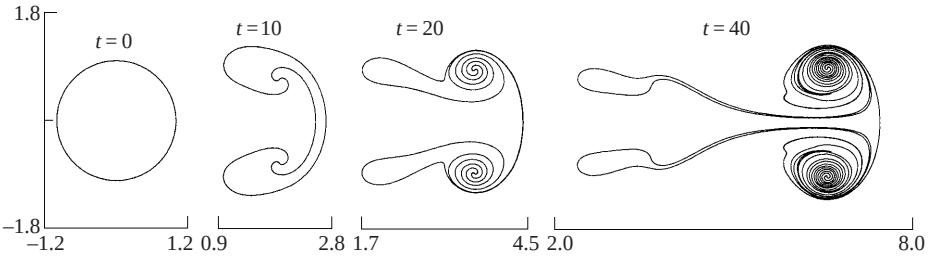

FIGURE 2. Computed axisymmetric solution at the indicated times, using $\delta = 0.2$.

travels, forming a vortex ring. The ring leaves a tail behind that is quite different from the planar tail. The lip observed at $t = 20$ is much longer than the planar one and is not entrained back into the leading ring. By $t = 40$, it forms a tail that is clearly separated from the main vortex and contains about 30% of the total circulation. Thus, the axisymmetric flow displays significant vortex shedding not present in the planar case. This indicates that the planar vortex pair entrains a larger region of fluid in the symmetry plane than the axisymmetric ring. In the planar case, this region appears to include the initial sheet while it only includes a portion of the initial sheet in the axisymmetric case. The fact that a vortex pair entrains a larger region of fluid than a vortex ring generated from similar initial conditions can also be observed in simulations by Krasny & Nitsche (2000), who computed the evolution of initially flat vortex sheets.

The beginning of the axisymmetric vortex shedding was observed in three-dimensional computations by Winckelmans *et al.* (1995). Figure 3 shows the further evolution of the axisymmetric vortex sheet roll-up. At $t = 60$, the vorticity in the tail of the leading vortex ring V_1 has rolled up into a second vortex ring V_2. Notice that at $t = 60$, V_2 has a tail that is similar to that of V_1 at $t = 20$, but smaller. This suggests a repetition of the shedding process in a self-similar manner at a smaller and smaller scale. Indeed, the tail of V_2 rolls up into a vortex V_3 ($t = 140$), which sheds a tail that rolls up into a vortex V_4 ($t = 350$), which sheds a tail that rolls up into a vortex V_5 ($t = 500$), apparently *ad infinitum.*

A detail of the computation remains to be explained. The leading vortex V_1 contains most of the circulation and therefore travels faster than the remaining vortices. At $t = 100$, it is several ring diameters ahead of the tail vorticity. In order to follow the shedding process to large times, V_1 was replaced at $t = 120$ by a circular vortex filament of equal circulation and impulse. This was found not to affect the local dynamics of the tail vorticity. Similarly, at $t = 300$, V_2 was replaced by a circular vortex filament. As part of this process the folds of the outer vortex sheet turns, seen for example on V_1 at $t = 100$ and on V_2 at $t = 240$, were also removed. As in the planar roll-up, these folds contain almost no vorticity and do not affect the dynamics of the remaining vortices.

To investigate how the observed planar and axisymmetric shedding behaviour depends on the regularization of the flow by δ, figure 4 plots the solution at a fixed time, computed with decreasing values of $\delta = 0.2$, 0.1, 0.05, with the planar case at $t = 50$ in the left column and the axisymmetric case at $t = 30$ in the right column. Both the vortex sheet ($y > 0$) and the associated regularized vorticity ($y < 0$), computed as the negative Laplacian of the streamfunction (2.5), are shown. The vorticity contours decrease by factors of 2, so that approximately equally spaced contours reflect an

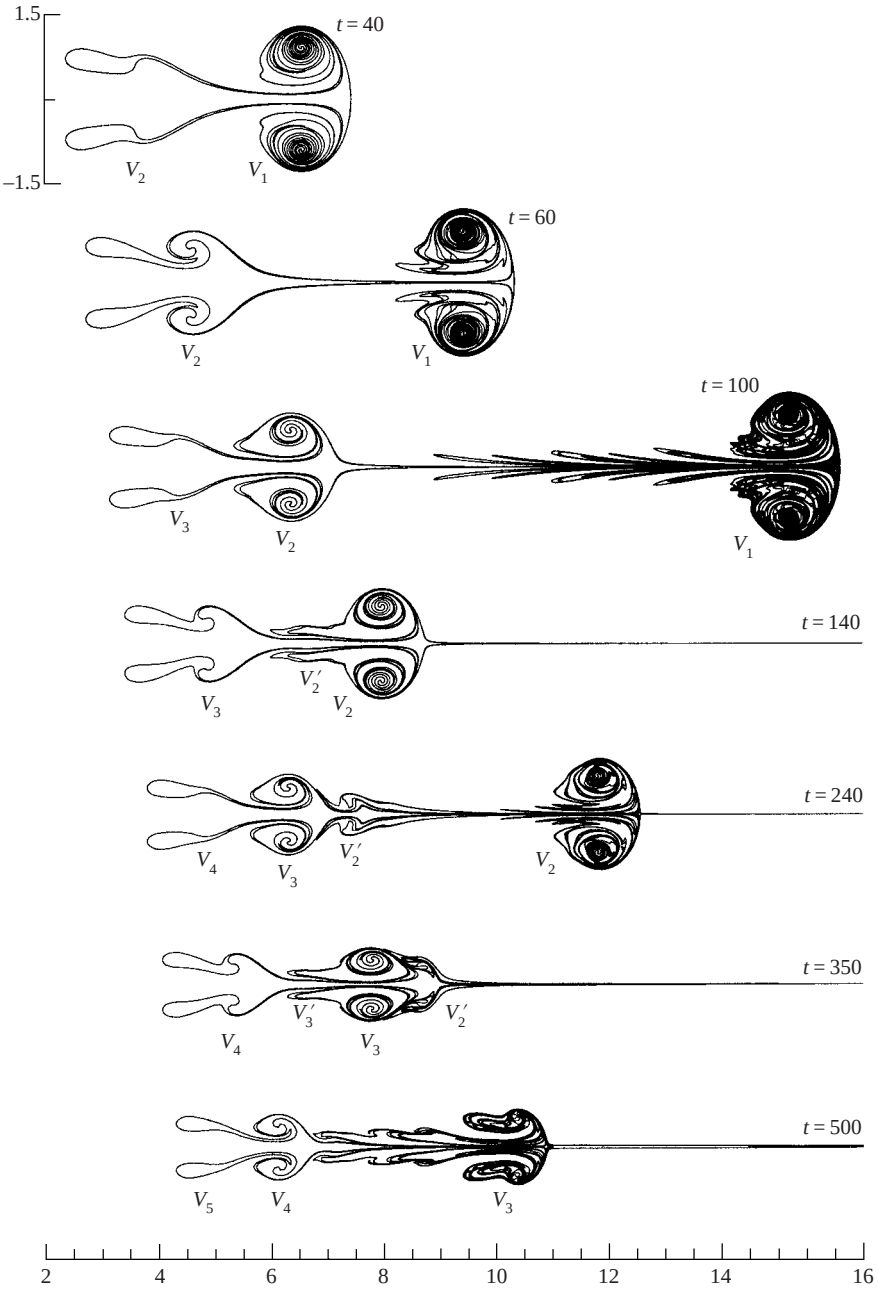

FIGURE 3. Computed axisymmetric solution at the indicated times, using $\delta = 0.2$. At $t = 120$, vortex V_1 is replaced by a circular vortex filament. At $t = 300$, vortex V_2 is replaced by a circular vortex filament.

exponentially decaying vorticity distribution. The largest contour level is $\omega = 2, 4, 8$ for $\delta = 0.2, 0.1, 0.05$ respectively. The smallest contour level is $\omega = 2^{-8}$.

The figure shows that the planar and axisymmetric shedding properties do not change much with δ. The vorticity has local maxima at the centre of the leading vortex and in the tail vorticity. As δ decreases, the maximum vorticity increases, the

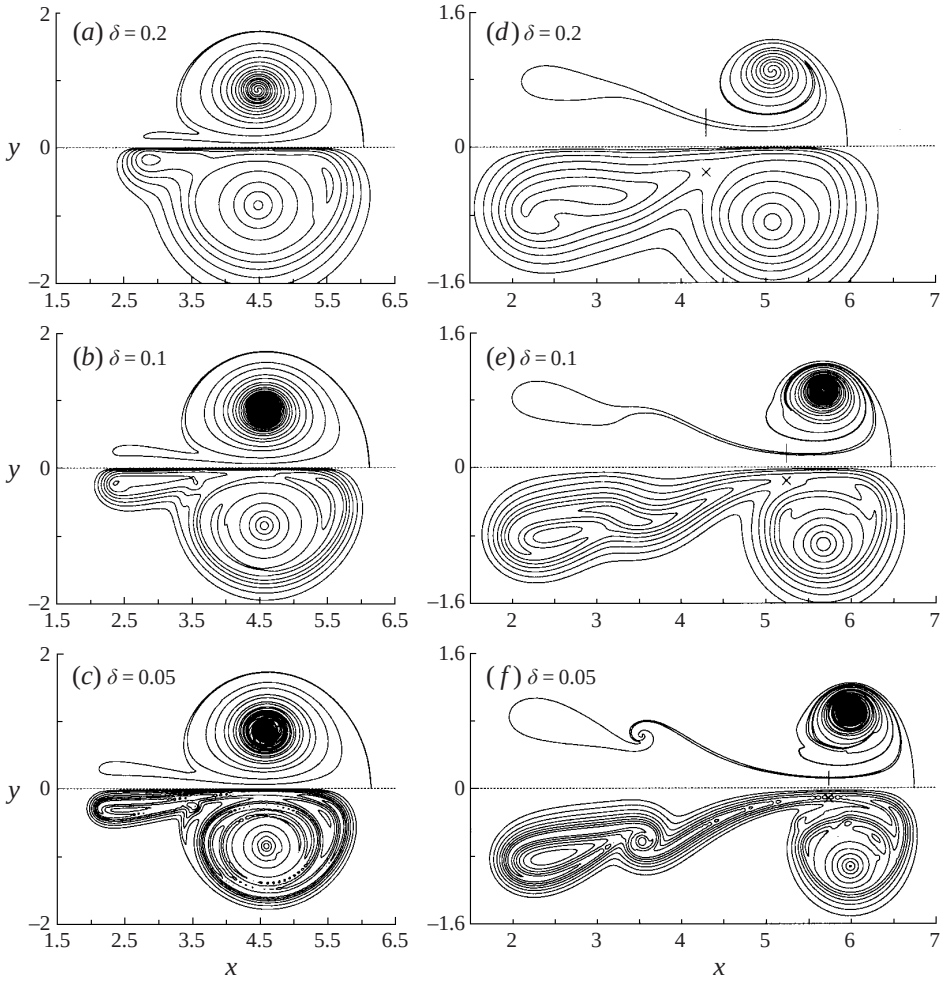

FIGURE 4. Vortex sheet ($y > 0$) and vorticity contours ($y < 0$) computed with the indicated values of δ. (a–c) Planar, $t = 50$. (d–f) Axisymmetric, $t = 30$.

contour levels steepen, and the vortex sheet roll-up tightens, but the total amount of circulation in the tail depends little on δ. It increases from 26% to 32% in the axisymmetric case and from 5.5% to 7% in the planar case. As noted earlier, in the planar case most of the tail vorticity is entrained by the leading vortex at later times, with only 1.5% of the total circulation remaining in the tail at $t = 150$ for $\delta = 0.2$. As δ decreases, the length of the planar tail increases (see figure 4a–c), and thus the portion that is not eventually entrained may possibly be bigger than 1.5%. The fact remains that independently of δ the axisymmetric vortex sheds a significant amount of circulation, approximately 30%, whereas the planar one sheds very little if any.

3.2. *Self-similarity of the shedding process*

The axisymmetric shedding process is slightly more complex than described so far. The leading vortex V_1 sheds a smaller vortex V_2 which in turn sheds a vortex V_3, and this process appears to repeat itself. However, after shedding the vortex V_3, V_2 sheds another amount of vorticity, V_2', as seen in figure 3 ($t = 140$). This vorticity

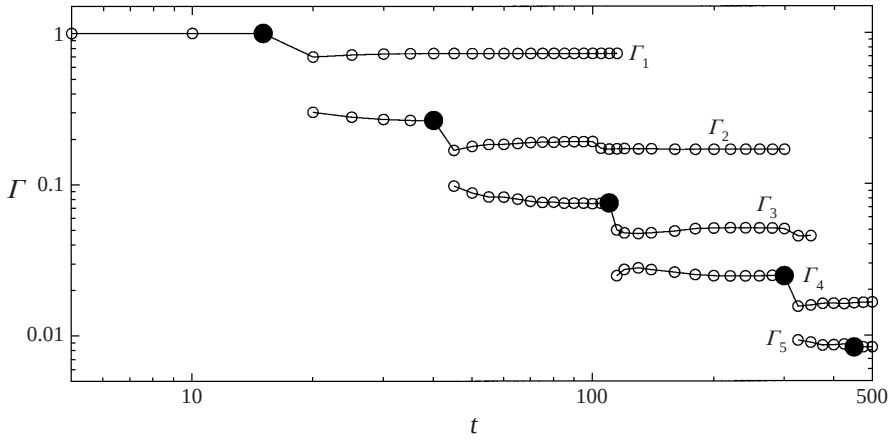

FIGURE 5. Circulation $\Gamma_n(t)$ of the nth vortex as a function of time t, $n = 1, \ldots, 5$.

rolls up slowly ($t = 240$) and does not form a well-defined vortex ring. The amount of vorticity in V_2' is much smaller than in the previously released vortex V_3. Thus V_3 travels faster than V_2' and soon catches up with the slower vortex ($t = 350$). Due to the interaction between V_2' and V_3 it soon becomes difficult to distinguish between them ($t = 500$) and the vortex evolution becomes less clear.

Note that this second shedding process just described also appears to repeat itself. At $t = 350$, V_3 is seen to shed a second amount of vorticity V_3', whose shape is similar to V_2' at $t = 140$. Soon after $t = 500$, V_3' will interact with V_4. V_4 in turn is expected to shed a second vortex V_4' which will interact with V_5, etc.

To investigate the apparent self-similarity of the shedding process, we first define the circulation of consecutive vortices V_n. Each vortex corresponds to a different vorticity maximum. The contours in figure 4 show that consecutive vorticity maxima are separated by saddle points in the vorticity distribution. The vortex V_n is defined as the portion of the vortex sheet about the nth maximum approximately delimited by saddle points. As an example, the crosses in figure 4(*d–f*, bottom half) denote saddle points; the vertical line segments in figure 4(*d–f*, top half) denote the limit between vortices V_1 and V_2. Once the portion of the sheet corresponding to V_n is determined, its circulation Γ_n is defined by

$$\Gamma_n = \int_{\mathbf{x}\in V_n} \omega \, \mathrm{d}A \approx \sum_{\alpha_j \in V_n} \Gamma'(\alpha_j)\Delta\alpha_j. \tag{3.1}$$

Figure 5 plots Γ_n as a function of time on a log-log scale. The open and solid circles denote the times at which the data is evaluated. Each value of Γ_n decreases when the next vortex with circulation Γ_{n+1} is shed. The values of Γ_2 and Γ_3 decrease slightly again at the time when the secondary vortices with circulation Γ_2' and Γ_3' are shed. It is interesting to observe that these secondary vortices V_2' and V_3' are shed at approximately the same time as V_4 and V_5, although no relation between these events is known. We remark that it is not easy to determine the exact time at which a new vortex is shed. The displayed shedding times simply reflect a time when a new saddle point has clearly formed between two vorticity maxima.

Figure 6(*a*) plots the circulation Γ_n of the nth vortex after it is well separated from the previous vortex, but before it has shed any further vorticity, that is, the values of Γ_n at the times t_n marked by solid circles in figure 5. The five data points in

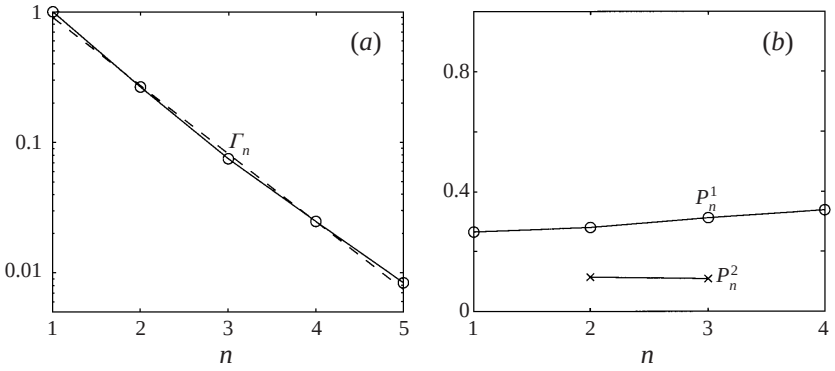

FIGURE 6. (*a*) Circulation of the *n*th vortex before shedding any further vorticity (solid line). Linear approximation (dashed line). (*b*) Percentage circulation $P_{n,1}$ and $P_{n,2}$ shed by the *n*th vortex the first and the second time respectively.

figure 6(*a*) are almost colinear on a semi-logarithmic scale. The dashed line has slope -1.2. Therefore $\Gamma_n(t_n)$ decays as

$$\Gamma_n(t_n) \sim \gamma^{-n} \tag{3.2}$$

with $\gamma = \mathrm{e}^{1.2}$, implying that each vortex sheds approximately $1/\gamma = 30\%$ of its circulation into its tail. This is confirmed by figure 6(*b*), which plots the percentage circulation $P_{n,1}$ of V_n that is shed into V_{n+1} and shows that it equals approximately 30% for all *n*. Figure 6(*b*) also plots the percentage $P_{n,2}$ of the remaining circulation of V_n that is shed into V_n'. Here, the only two data points available are for V_n, $n = 2, 3$. Each sheds about 10% into V_n'.

Furthermore, the time that it takes for V_n to shed V_{n+1} also appears to follow a power law. Note that the vortex V_n is formed at time t_{n-1} and sheds the next vortex V_{n+1} at time t_n, for $n = 2, \ldots, 4$. The time $t_n - t_{n-1}$ appears to increase as $1/\Gamma_n$,

$$t_n - t_{n-1} \sim \gamma^n. \tag{3.3}$$

To illustrate this, figure 7 plots $\Gamma_n^* = \gamma^n \Gamma_n$ vs. $t_n^* = (t - t_{n-1})/\gamma^n$, for $n = 2, \ldots, 5$. The value $n = 1$ is excluded since V_1 did not arise through shedding and therefore t_1^* is not defined. Each curve in the figure corresponds to a different value of *n*. All curves almost collapse onto one curve, giving evidence that the scaling laws (3.2) and (3.3) are fairly well satisfied. Equation (3.3) holds since each vortex V_n, for $n = 2, \ldots, 4$, sheds the next vortex V_{n+1} at aproximately the same time $t^* = 2$, thus showing that $(t_n - t_{n-1})/\gamma^n$ is approximately constant. Notice that the second vortex shedding of V_n', for $n = 2, 3$, also occurs at approximately the same time $t^* = 7.5$. The non-dimensional timescale therefore appears to be proportional to $\Gamma_n(t - t_{n-1})$. The length scale used in this non-dimensionalization is the initial radius *a*. One would however suspect that the appropriate length scale would be a characteristic size a_n of the *n*th vortex. The reason that this does not work as well may be due to the fact that there is another parameter in the numerical experiment, δ/a_n, which varies from vortex to vortex.

3.3. *On Kelvin's energy principle*

We now relate the observed shedding to a variational principle due to Lord Kelvin. For planar vortices in a steady state, the kinetic energy is at a local extremum with respect to perturbations that preserve the circulation of fluid elements and the total impulse (Saffman 1992, § 14.2). For axisymmetric axis-touching vortex rings, the

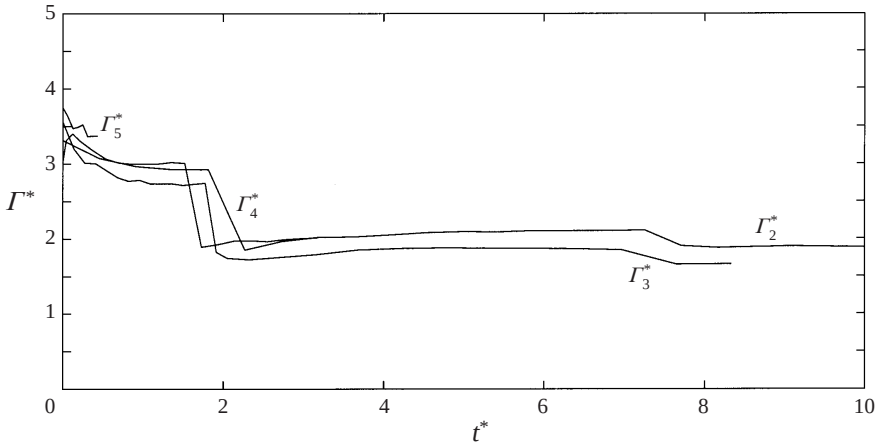

FIGURE 7. Scaled circulation Γ_n^* of the nth vortex as a function of scaled time t_n^*, $n = 2, \ldots, 5$.

steady states are expected to occur at local maxima of the kinetic energy (Kelvin 1880; Benjamin 1976). Gharib *et al.* (1998, referred to as GRS) and Mohseni & Gharib (1998) applied this principle to explain observations in experiments in which a vortex ring was formed by ejecting fluid from the edge of a tube. GRS observed that the ring circulation could not be made as large as desired by simply continuing to eject fluid from the tube. After a critical value of the piston stroke, the ejected circulation was no longer absorbed by the leading ring but formed secondary vortices in its tail. GRS showed that the leading ring's circulation stopped increasing when the rate at which circulation, impulse and energy were ejected was too small to maintain the energy of the ring. They considered a normalized energy that scaled out variations in circulation and impulse. The results are consistent with the premise that the ring had reached a local energy maximum and corresponding steady state. GRS also observed that rings which had gained excess circulation through entrainment reduced it by vortex shedding. They conjectured that such shedding would occur for rings whose energy is too small to sustain a steady state.

Here, we investigate the relation between the present vortex shedding and the energy of the vortices. Following GRS, each vortex V_n is normalized with respect to its total circulation and impulse. The corresponding non-dimensional energy E_n is

$$E_n = \frac{K_n}{\Gamma_n^{3/2} I_n^{1/2}}, \tag{3.4}$$

where the kinetic energy K_n and impulse I_n are

$$K_n = \pi \int_{\substack{\mathbf{x}\in V_n \\ y\geqslant 0}} \psi\, \omega \, \mathrm{d}A \approx \pi \sum_{\alpha_j \in V_n} \psi(x_j, y_j, t)\, \Gamma'(\alpha_j)\, \Delta\alpha_j, \tag{3.5}$$

$$I_n = \pi \int_{\substack{\mathbf{x}\in V_n \\ y\geqslant 0}} y^2\, \omega \, \mathrm{d}A \approx \pi \sum_{\alpha_j \in V_n} y_j^2\, \Gamma'(\alpha_j)\, \Delta\alpha_j. \tag{3.6}$$

Figure 8 (solid curves) plots E_n vs. t for the computations shown in figures 2 and 3. Comparison with figure 5 shows that each time V_n sheds a vortex, its non-dimensional energy E_n increases. The values of E_2 and E_3 increase twice, since the corresponding vortices shed vorticity twice. After this second increase, no more significant energy

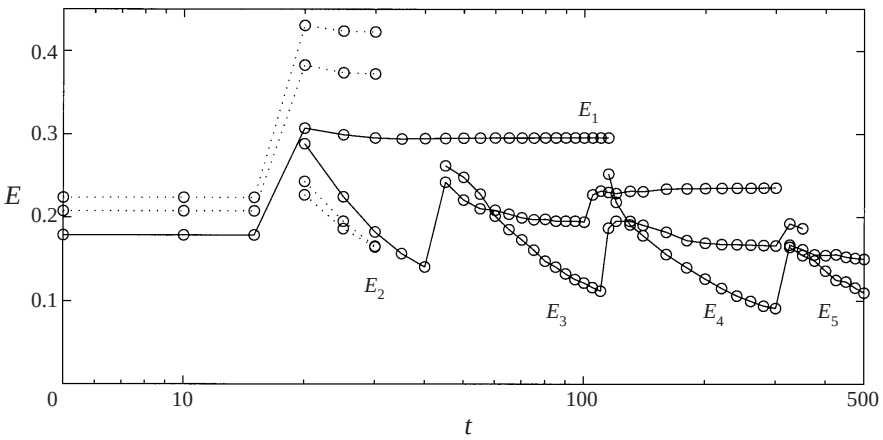

FIGURE 8. Non-dimensional energy E_n of the nth vortex vs. time, for computations with $\delta = 0.2$ (solid line) and $\delta = 0.1, 0.05$ (dotted line).

increase and corresponding vortex shedding is expected. Notice that the values of E_2–E_4 decrease before the first vortex shedding, instead of being constant as they would for an isolated vortex. This is attributed to the proximity of neighbouring vortices shortly after shedding and associated transfer of impulse and energy.

We interpret these data as follows. The initial spherical vortex is not at a steady state and its non-dimensional energy is far from a local maximum. As conjectured by GRS, this results in circulation shedding, which causes the vorticity distribution within the vortex to change so that its non-dimensional energy increases. Presumably, with each shedding the energy approaches a local maximum and the corresponding vortex approaches a steady state. The process repeats itself for the subsequent vortices.

The values of the computed energy E depend on the regularization by δ. The dotted curves in figure 8 show the results for computations with $\delta = 0.1$ and 0.05 on a small time interval on which they could be resolved. As δ decreases, the initial value of E_1 converges to the exact value for the unregularized spherical vortex sheet, $\frac{1}{3}\sqrt{\pi/6} \approx 0.24$. The value of E_1 at late times appears to increase to approximately 0.45 as δ decreases. The values of E_2–E_5 at late times when no more shedding occurs are expected to be all equal, since the corresponding vortices appear to be self-similar. However, in figure 8, these values decrease with n. This is attributed to the increasing values of δ for each vortex, relative to the vortex size. It is expected that in the limit $\delta \to 0$ the late time values of E_n, $n \geqslant 2$, are all equal.

The long-term steady vortex rings observed by GRS have non-dimensional energy $E \approx 0.33$. Norbury (1973) computed a family of steady vortex rings with varying mean core radius $0 \leqslant r_c \leqslant \sqrt{2}$ for which $0.16 \leqslant E \leqslant \infty$, where E increases as r_c decreases. The present vortex V_1 therefore has different energy E at late times than GRS's steady ring, which implies that it has a different vorticity distribution. It has the same energy as a Norbury vortex with $r_c \approx 0.3$. It is not clear how the late-time values of E_2–E_5 compare with the value observed by GRS.

4. Summary

The roll-up of a cylindrical and a spherical vortex sheet into a vortex pair and a vortex ring respectively was computed with the vortex blob method. The vortex pair travels downstream leaving almost no vorticity behind. In contrast, the vortex ring

sheds about 30% of its circulation into a tail. This shedding process repeats itself in a self-similar manner: each tail rolls up to form a new ring which sheds 30% of its circulation into a new tail. The time interval between formation and shedding is proportional to the inverse of the rings' circulation. Each ring except the leading one appears to undergo a second shedding of about 10% of its remaining circulation. With each shedding, the non-dimensional energy of the vortex rings increases and presumably approaches a local maximum at which the rings translate steadily. The shedding process is therefore viewed as a mechanism by which the rings approach a steady state.

I thank Vachtang Putkaradze and Karim Shariff for helpful comments. This work was supported by NSF grant DMS-9996254.

REFERENCES

Anderson, C. R. 1985 A vortex method for flows with slight density variations. *J. Comput. Phys.* **61**, 417–444.

Batchelor, G. K. 1967 *An Introduction to Fluid Dynamics*. Cambridge University Press.

Benjamin, T. B. 1976 An alliance of practical and analytical insights into the non-linear problems of fluid mechanics. In *Applications of Methods of Functional Analysis to Problems in Mechanics* (ed. P. Germain & B. Nayroles). Lecture Notes in Mathematics, vol. 503, pp. 8–28. Springer.

Chorin, A. J. & Bernard, P. S. 1973 Discretization of a vortex sheet, with an example of roll-up. *J. Comput. Phys.* **13**, 423–429.

Gharib, M., Rambod, E. & Shariff, K. 1998 A universal time scale for vortex ring formation. *J. Fluid Mech.* **360**, 121–140 (referred to herein as GRS).

Kelvin, Lord 1880 Vortex Statics. *Phil. Mag.* **10**, 97–109.

Krasny, R. 1986 Desingularization of periodic vortex sheet roll-up. *J. Comput. Phys.* **65**, 292–313.

Krasny, R. 1987 Computation of vortex sheet roll-up in the Trefftz plane. *J. Fluid Mech.* **184**, 123–155.

Krasny, R. & Nitsche, M. 2000 The onset of chaos in vortex sheet flow. *J. Fluid Mech.* (submitted).

Mohseni, K. & Gharib, M. 1998 A model for universal time scale of vortex ring formation. *Phys. Fluids* **10**, 2436–2438.

Nitsche, M. & Krasny, R. 1994 A numerical study of vortex ring formation at the edge of a circular tube. *J. Fluid Mech.* **276**, 139–161.

Norbury, J. 1973 A family of steady vortex rings. *J. Fluid Mech.* **57**, 417–431.

Rottman, J. W., Simpson, J. E. & Stansby, P. K. 1987 The motion of a cylinder of fluid released from rest in a cross-flow. *J. Fluid Mech.* **177**, 307–337.

Rottman, J. W. & Stansby, P. K. 1993 On the 'δ-equations' for vortex sheet evolution. *J. Fluid Mech.* **247**, 527–549.

Saffman, P. G. 1992 *Dynamics of Vortex Flows*. Cambridge University Press.

Tryggvason, G., Dahm, W. J. A. & Sbeih, K. 1991 Fine structure of vortex sheet roll-up by viscous and inviscid simulation. *Trans. ASME: J. Fluids Engng* **113**, 31–36.

Winckelmans, G. S., Salmon, J. K., Leonard, A. & Warren, M. S. 1995 Three-dimensional vortex particle and panel methods: fast tree-code solvers with active error control for arbitrary distributions/geometries. In *Proc. Forum on Vortex Methods for Engineering Applications, Albuquerque, NM, February 1995*, pp. 25–43. Sandia National Laboratories.